Large Space Telescope Oscillations Induced by CMG Friction

S. M. Seltzer*
NASA Marshall Space Flight Center, Ala.

The major objective of this investigation is to predict conditions under which limit cycles may be caused by the friction torque of the CMG output gimbal used in the Large Space Telescope (LST). Because of the uncertainty surrounding the precise nature of the nonlinearity, three different portrayals are used. The relative fidelity of the three models is discussed, as is their similarities and differences. The investigation is analytical in nature, using describing functions to describe the friction nonlinearities. Stable regions of operation are determined on a selected two-parameter plane. The conditions under which limit cycles will exist are determined on that plane, and their characteristics (amplitude and frequency of oscillation) are predicted.

Nomenclature

A = limit cycle amplitude
A_0, A_1 = vehicle attitude control gains for Model 3
$\bar{A}_1, \bar{B}_1$ = numerator of N_1 and N_2, respectively
a = $\equiv 2_\gamma A T_{GFo}$
D = dead zone
$f(x)$ = assumed sinusoidal output of nonlinearity N
$G(s)$ = general form for transfer function representing linear portion of overall plant
$G_G(s)$ = general form for transfer function representing linear portion of CMG
H = angular momentum
I_{GE} = CMG gimbal effective moment of inertia
I_v = vehicle moment of inertia
i = designated imaginary component
J = Jacobian
K = $\equiv (4T_{GFo})^{2/3}\gamma^{1/2}/\Pi$
K_0, K_1 = vehicle attitude control gains (weighted for Model 3)
K_I, K_p = CMG gimbal rate control gains for Dahl model
K_G, g_0, g_1 = characteristic parameters of second order model of CMG
k = primary slope of Model 1 nonlinearity
k_F = CMG feedback gain for Model 1
k_T, k_γ = multiplication factors associated with T_{GFo} and γ, respectively
M = relay gain
m = secondary slope of Model 1 nonlinearity
N = nonlinear gain, characterized herein as a describing function
N_1 = real part of Dahl model describing function
N_2 = imaginary part of Dahl model describing function
$R(s)$ = attitude rate sensor transfer function
s = complex variable (Laplace operator)
T_c = torque command to vehicle
T_f = CMG output gimbal pivot frictional torque
T_{GFo} = running friction torque
T_{OA} = torque response of vehicle
t = time
u = $\equiv D/A$
x = sinusoidal input to nonlinearity N
y = $\equiv dT_f/d\theta$
ln = natural logarithm
$\mathfrak{L}$ = $\equiv 2a^2+2a+1$
Ω = imaginary part of s associated with system frequency; as used herein, also limit cycle frequency of oscillation
α, β = weighted vehicle control gains for Model 1
γ = CMG gimbal pivot friction parameter
δ = CMG output gimbal angle
$\dot{\delta}$ = CMG output gimbal angle rate
$\dot{\delta}_c$ = commanded CMG output gimbal angle rate
ζ_{CMG} = damping ratio of CMG
θ = vehicle attitude
κ_0, κ_1 = CMG control gains Model 2
ξ = $\equiv Dk/M$
σ = $\equiv \gamma T_{GFo}^2$
ϕ = phase shift from x to $f(x)$
χ = commanded vehicle attitude
ω = imaginary component of s (identified with frequency)
ω_c = bandwidth of first order model of CMG
ω_g = bandwidth of first order model of attitude rate sensor
$\omega_n]_{CMG}$ = natural frequency of CMG
= derivative with respect to time

Received May 6, 1974; revision received October 10, 1974.
Index categories: Spacecraft Attitude Dynamics & Control; Navigation, Control and Guidance Theory.

*Chief, Pointing Control Systems Branch, Systems Dynamics Laboratory. Associate Fellow AIAA.

Introduction

THE nature of the control moment gyroscope (CMG) output gimbal bearing friction has been the subject of many discussions and presentations by various investigators. It is important to know the precise nature of the torque caused by the bearing friction so that its effect on the dynamic behavior of the Large Space Telescope (LST) and its pointing and control system (PCS) can be predicted. The objective of the analysis and supporting computer simulations reported herein is to study the effect of the assumed CMG nonlinearity upon the system dynamics in order to develop an understanding of the nature and effect of variations of numerical values of parameters upon the system.

Three separate models of the CMG output gimbal bearing friction are used in three separate analyses. Model 1 is included primarily for historical reasons, since subsequent research has indicated that it probably is an incorrect portrayal of the actual physical phenomenon. However, variations of it are still found in current literature.[1] Consequently it is included herein. Models 2 and 3 are similar in nature and are both currently being used for analysis. As will be seen, Model 2 is nearly a piecewise-linear simplification of Model 3. Because experimental results now underway imply the adequacy of their use in modeling the physical phenomenon of gimbal bearing friction, they are both included in the analyses reported upon herein. The purpose of

performing these analyses is to predict under what conditions limit cycles will be caused by the nonlinear representation of this friction characteristic. The weakness of the mathematical analysis used results from the need to restrict the complexity of the models studied; however, the design insight obtained is valuable.

The parameter plane analysis technique used herein makes use of the describing function to portray the nonlinearity representing CMG gimbal bearing friction. Where the describing function is a complex value, the technique developed for a system containing two nonlinearities may be applied.[2] This technique affords both analytic and graphic portrayal of the effects of variations in selected system parameters. With few exceptions (noted herein) the results are confirmed with analogue computer simulation.

Finally, the reader is cautioned against relying solely on computer simulations without adequate mathematical analysis as a background. An attempt to use an analogue computer to define stability boundaries for satellite dynamics as characterized by the Mathieu equation would convince even the skeptic of the weakness of computer simulation when not augmented by mathematical analysis. A current example in the field of digital simulation is the errors (apparently introduced by computer mechanization) contained in Connell's paper[3] reported by Schiehlen[4]. The following three models are considered in this report and are analyzed in detail:

Model 1. A single axis representation of the model developed by the Bendix Corporation and presented to George C. Marshall Space Flight Center (MSFC) in April 1972.[5–7]

Model 2. A modification of the Sperry model presented to MSFC in December 1972.

Model 3. The model developed by P. R. Dahl of Aerospace Corporation (the so-called Dahl Model). This model also may be incorporated into a single-axis representation.

Analysis Technique

The objective of the analyses presented herein is to determine general stability conditions and, in particular, conditions under which limit cycles may occur for systems that may be represented schematically, as in Fig. 1. The plant under consideration is represented by a linear part *G(s)* and a nonlinear element *N*. In the sequel *N* will be used to represent the nonlinear friction characteristics of the CMG gimbal pivot. In particular it is of interest to investigate the possibility of existence of limit cycles and to determine their characterisitics. As used herein the term "limit cycle" will be used synonomously with the term "self-excited sustained oscillation." Hence, a limit cycle represents a steady-state oscillation to which or from which all neighboring trajectories in a state space will converge or diverge.[8,9]

Because of the low-pass nature of the linear parts of the system plants under consideration, they are particularly amenable to analysis through application of describing function theory. Hence a discussion of appropriate describing functions is needed.[10] It is assumed that, if a sustained oscillation occurs, the input x to the nonlinearity is described by

$$x = A \sin \Omega t \tag{1}$$

It is assumed that the nonlinearity's output *f(x)* is approximated by the relation

$$f(x) \approx NA \sin(\Omega + \phi)t \tag{2}$$

where ϕ represents a phase shift.

Because the precise nature of the relationship between the input *(x)* to the nonlinear element *(N)* of the CMG model and the output *f(x)* still is obscure, the effect of variations of the parameters describing that relationship is studied. In particular it is desired to predict whether or not sustained

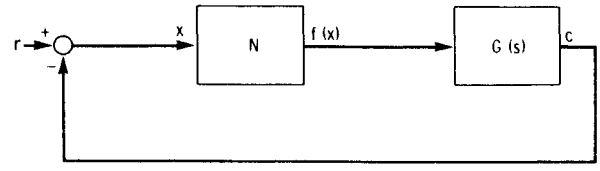

Fig. 1 Basic nonlinear system.

oscillations in the vehicle's attitude and attitude rate will occur and, if so, what their characteristics are (in terms of amplitude, period, and stability) under various prescribed conditions.

The method of analysis used is defined in Ref. 2 and embodies a describing function technique developed by Siljak.[11] It is assumed that the system being analyzed is amenable to describing function analysis and the system parameters are time-invariant. In essence, a describing function *(N)* is used to represent the nonlinearity. The characteristic equation representing the system is then obtained. For a limit cycle to occur, it is required that all characteristic equation roots have negative real parts except for one pair of roots which must be purely imaginary roots. This condition is determined mathematically and for ease of visualization may be portrayed graphically. In the latter case, two adjustable parameters are selected, at least one of which must also contain *N*. (If *N* is a complex quantity, its real and imaginary-components may be used as the two parameters and Ref. 2 may be applied directly.) A correlation between these parameters and the roots of the characteristic equation is then determined by mapping stability contours from the complex s-plane onto the chosen parameter plane. For the systems considered herein, only three (and sometimes fewer) such stability boundaries exist and they are easily found.

The first boundary (the one associated with real roots of the characteristic equation) is found by setting $s=0$ in the characteristic equation. (Graphically this boundary may be identified by single hachures.) The second one (the one associated with purely imaginary roots) is found by setting $s=j\omega$. (This boundary is identified by cross-hachures.) The third one, called the boundary at infinity (in topological mapping from the complex *s*-plane to the Riemann sphere, it is associated with the sphere's north pole), is found by setting $1/s=0$ in the characteristic equation. It also is identified by single hachures. From these boundaries, the stable region (if it exists) may be determined in terms of the selected adjustable parameters, for they bound the stable region.

The nonlinear locus of *N* as a function of the two adjustable parameters is determined next. The simultaneous solution of the nonlinear locus relation and the purely imaginary root boundary yields the condition for a limit cycle, assuming the indicated solution occurs adjacent to a stable region (which may not always be the case). This is readily apparent on the parameter plane as the intersection between the purely imaginary root boundary and the nonlinear locus. From this point of intersection, the frequency (identified as $\omega=\Omega$) and magnitude *(A)* of an indicated limit cycle may be determined as a function of characteristics of the nonlinearity and of the adjustable parameters. Further, the behavior of the limit cycle when a small perturbation is applied to its amplitude, and, hence, the nature of limit cycle stability, also is apparent on the parameter plane.

Analysis of Model 1

The model is characterized as a single axis representation of a CMG, a rate gyro, and rigid body dynamics (Fig. 2). The CMG is modeled as a nonlinear element *N* and a second-order transfer function

$$G_G(s) = K_G(s^2 + g_1 s + g_0) \tag{3}$$

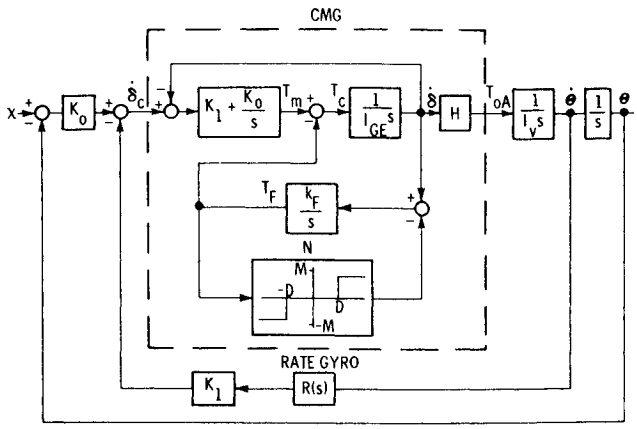

Fig. 2 Model 1.

The addition of an imperfect attitude rate sensor, described by a first order transfer function

$$R(s)=\omega_g/(s+\omega_g) \tag{4}$$

increases the order of the characteristic equation by one (beyond the order of the characteristic equation with an assumed perfect sensor). The characteristic equation is

$$s^5+(g_1+\omega_g)s^4+(g_0+\omega_g g_1)s^3 +\omega_g g_0 s^2+(\omega_g\beta+\kappa)Ns +\omega_g\kappa N=0 \tag{5}$$

where

$$\alpha\equiv K_0K_G/I_v \tag{6a}$$

and

$$\beta\equiv K_1K_G/I_v \tag{6b}$$

The stable region, in terms of an $\alpha N-\beta N$ parameter plane, is bounded by the real root boundary

$$\alpha N=0 \tag{7}$$

and the imaginary root boundary

$$\alpha N=\omega^2\{g_0-[1+(g_1/\omega_g)]\omega^2\} \tag{8a}$$

and

$$\beta N=g_1\omega^2(1+\omega^2/\omega_g{}^2) \tag{8b}$$

The nonlinear locus is the straight line determined by Eq. (8):

$$\beta N=(K_1/K_0)\alpha N \tag{9}$$

This is shown in Fig. 3. If a limit cycle is to occur, it will have the characteristics associated with the intersection of the boundary defined by Eqs. (8) and the nonlinear locus [Eq. (9)]. Using the numerical values of Table 1 to solve Eqs. (8) and (9) simultaneously leads to numerical values for N of 2.103 and Ω of 40.959 rad/S = 6.519 Hz. The frequency Ω of the indicated limit cycle is determined by system parameters and has the same value regardless of the type of nonlinearity chosen for N. Although the value of N is also independent of the type of nonlinearity, the amplitude A of the limit cycle is dependent on the relation between N and A, as in Eq. (11).

Some general characteristics may be deduced. If the nature of the nonlinearity is such that N increases monotonically as A increases, then an unstable limit cycle is indicated.

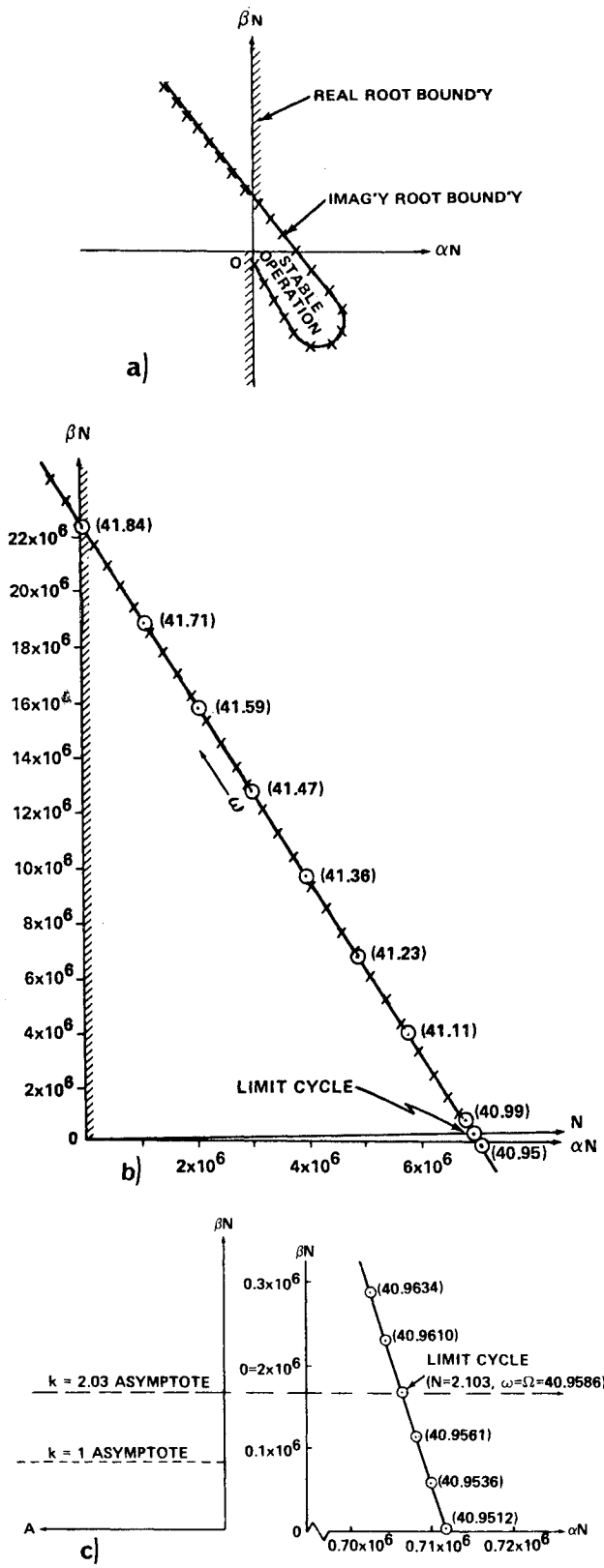

Fig. 3 Stability characteristics, Model 1. a) Sketch of overall characteristics; b) First quadrant view. c) Selected portion of first quadrant and βN vs A.

However, if N increases but approaches a limit asymptotically as A increases, the limit cycle will occur only if the asymptote has a value such that the nonlinear locus intersects the imaginary root stability contour. If N decreases monotonically as A increases, a stable limit cycle will occur as long as the nonlinear locus begins at a value sufficiently high

Table 1 LST Numerical values

Parameter	Numerical value
g_0	$=K_G=10^4$ (rad/sec)^2
g_1	141.4 rad/sec
H	610 Nmsec
I_{GE}	5.012 Nmsec^2 (3.7 ft-lb sec^2)
I_v	1.356×10^5 Nmsec^2
K_0	4.6843×10^6 Nm
K_1	1.1153×10^6 Nmsec
k_F	6.600×10^3 Nm/rad
ζ_{CMG}	0.707
κ_0	4.352×10^4 $(=\omega_n^2 I_G - k_f)$
κ_1	7.087×10^4 $(=2\zeta\omega_n I_G)$
ω_g	30 rad/sec
$\omega_n]_{CMG}$	100 rad/sec

that an intersection occurs with the stability contour. If the nonlinear locus remains above the stability contour for all A no limit cycle will occur. These observations lead to an investigation of describing function characteristics for various appropriate nonlinearities.

If the nonlinearity portrayed in Fig. 2 is considered and the small overshoots occurring at $x=D$ and $x=-D$ are ignored, the describing function is

$$N/k=1-(2/\pi)\{(1-(m/k)\sin^{-1}u+[1-(2/\xi)-(m/k]u(1-u^2)^{1/2}\},u<1 \quad (10a)$$

$$N/k=m,u> \quad (10b)$$

For small values of m ($m\ll k$), the relation approximated by the describing function defined in Eqs. (10) then becomes

$$N/k=1-(2/\pi)\{\sin^{-1}u+[1-(2/\xi)]u(1-u^2)^{1/2}\},u\le1 \quad (11a)$$

$$N/k=0,\ u>1 \quad (11b)$$

where

$$u\equiv(D/A) \quad (12a)$$

and

$$\xi\equiv(DK/M) \quad (12b)$$

Further study of the describing function reveals the amplitude of the peak value of N/k and the values of ξ and u (and hence D, M, and k) for which the peak occurs. If Eq. (10a) is optimized with respect to u, it is found that the peak value, N_0/k, of N/k occurs when u has the value

$$u_0=[(\xi-1)/(\xi-2)]^{1/2} \quad (13)$$

The effect of varying the basic nonlinearity's parameters k, M, and D will be investigated. An examination of Figs. 2 and 3 yields most of the following information:

Condition 1) $N>k>M/D$: Stable operation (no limit cycle).

Condition 2) $N<k<M/D>k/\xi_o$: Two limit cycles; one stable, one unstable with $A^u<A^s$.

Condition 3) $N>k<M/D<k/\xi_0$: Stable operation (no limit cycle).

Condition 4) $N<k>M/D$: Unstable limit cycle.

Condition 5) $N<k<M/D$: Unstable limit cycle.

Condition 6) $N>k<M/D=k/\xi_0$:Semistable limit cycle.

Additional information was needed to obtain the inequality relationships between M/D and k/ξ_0 for Conditions 2, 3, and 6. From Eq. (13), it is seen that a peak in N/k vs A/D can occur only when

$$\xi>2 \quad (14a)$$

or

$$\xi<1 \quad (14b)$$

Since D/A must be less than unity for Eq. (11a) to be applicable, it is seen from Eq. (12a) that inequality (14a) is meaningless physically. Also from Eq. (11b), it is seen that $\xi>0$. To summarize, N/K will have a peak only when $0<\xi>1$ $(k<M/D)$ and will approach but not exceed the value of asymptote $N/k=1$ when $\xi>1$ $(k>M/D)$. Using values shown in Table 1, numerical examples corresponding to each of these six conditions are developed and summarized in Table 2. Attention is directed to the case covered by Condition 1 where-$M=D$, $k=1$: this is the set of conditions on the nonlinearity that is used in Refs. 5—7 and is reported as causing limit cycles. The analysis predicts stable operation and the absence of any limit cycles. Most of the results obtained from the above analysis and summarized in Table 2 have been confirmed by analog simulation.[12] Because the describing function technique assumes that the input and output to the nonlinearity are both sinusoidal in nature, it is to be expected that the actual magnitudes of these transcendental functions will only be approximated by the mathematical estimates. The

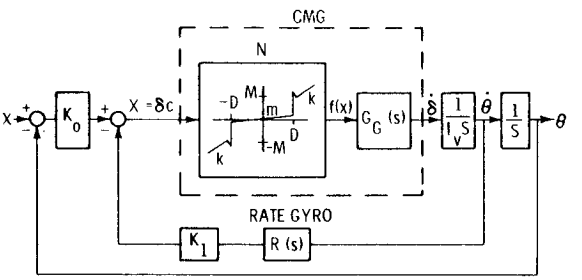

Fig. 4 Model 2.

Table 2 Summary of model 1 results[a]

Case	Condition	k	D	M	A(rad)	NA(rad)	θ_{LC}(rad)	$\dot\theta_{LC}$ (rad/sec)
1A	$N>K=M/D$	1	0.011	0.011	Stable Response			
1B	$N>k>M/D$	1.5	"	0.011				
2	$N>k<M/D>k/\xi_0$	2	"	0.044	0.0123^u	0.0258^u	1.1371×10^{-10}	1.1028×10^{-8}
					0.270^s	0.567^s	2.4961×10^{-9}	2.4209×10^{-7}
4	$N<k>M/D$	5	"	0.011	0.0188^u	0.0395^u	1.7380×10^{-10}	1.6856×10^{-8}
5	$N<k<M/D$	5	"	0.0825	0.01128^u	0.0237^u	1.0428×10^{-10}	1.01139×10^{-8}
6	$N>k<M/D$	1	"	1/0.16	$0.016^{u,s}$	$0.0336^{u,s}$	1.4792×10^{-10}	1.4345×10^{-8}

[a] In all runs, predicted and measured values of Ω were identical: $\Omega=6.519$ Hz. Superscripts u, s indicate values associated with unstable *(u)*, stable *(s)*, or semi stable *(u,s)* limit cycles.

closeness of the predictions to the simulation results was surprisingly accurate, considering the shape of the waveforms at the output of the nonlinearity. The predicted time periods were particularly accurate.

Analysis of Model 2

A brief analysis was made of the modification of the Sperry model that was presented to MSFC in Dec. 1972. The model that was presented was similar to that shown in Fig. 4 with the exception that the nonlinearity has an infinite gain at $\pm D$. This was modified to be a high gain M beginning at $\pm D$ to facilitate analysis and analog computer implementation. The characteristic equation associated with the model is

$$\frac{I_v I_{GE}}{k_F} s^5 + I_v \left(\frac{\kappa_1}{k_F} + I_{GE} N \right) s^4 + \left[I_v \left(\frac{\kappa_0}{k_F} + 1 + \kappa_1 N \right) + H K_1 \frac{\kappa_1}{k_F} \right] s^3 + \left[I_v \kappa_0 N + H K_1 \left(\frac{\kappa_0}{k_F} + \kappa_1 N \right) + H K_0 \frac{\kappa_1}{k_F} \right] s^2 + H \left[K_1 \kappa_0 N + K_0 \left(\frac{\kappa_0}{k_F} \kappa_1 N \right) \right] s + H K_0 \kappa_0 N = 0 \quad (15)$$

where N represents the CMG nonlinear element (gimbal pivot friction). If $1/k_F$ and N are selected as the two parameters of interest in the limit cycle and stability investigation, one obtains three stability boundaries. The real root boundary is

$$N = 0 \quad (16)$$

and the boundary at infinity is

$$1/k_F = 0 \quad (17)$$

The imaginary root boundary may be written as

$$1/k_F = -I_v \Omega^2 [I_v I_{GE} \Omega^4 - (I_v \kappa_0 + H K_1 \kappa_1) \Omega^2 + H K_0 \kappa_0] / J \quad (18a)$$

$$N = I_v \Omega^4 [I_v \kappa_1 \Omega^2 - H(K_0 \kappa_1 + K_1 \kappa_0)] / J \quad (18b)$$

where the Jacobian J of the simultaneous equations obtained from the real and imaginary parts of Eq. (15) is

$$J = -\Omega^2 [I_v \kappa_1 \Omega^2 - H(K_0 \kappa_1 + K_1 \kappa_0)]^2 - [I_v I_G \Omega^4 - (I_v \kappa_0 + H K_1 \kappa_1) \Omega^2 + H K_0 \kappa_0]^2 \quad (18c)$$

For the general case, the $1/k_F - N$ parameter plane stability plot takes the form of Fig. 5. The region of interest of this figure for limit cycle considerations is enlarged and plotted on Fig. 6. Shown in Fig. 4 is a sketch of the nonlinearity N of the model to which Eq. (11) with $k = 0$ applies. If the nonlinear locus N(as a function of A) is reflected from the describing function graph onto the parameter plane, it is seen to be a vertical line rising from (and returning to) $1/k_F$ as A increases positively. Thus if $1/k_F > 1.6 \times 10^{-7}$ ($k_F < 8.62 \times 10^6$), no limit cycle can occur. If $1/k_F < 1.16 \times 10^{-7}$, then zero, two, or four limit cycles are predicted, depending on whether the peak value of $ND/M(=2/\pi)$ intersects with none, one, or both of the portions of the complex root boundary. From Table 1 it is seen that the nominal value of k_F is 6600 ($1/k_F = 1.52 \times 10^{-4}$), indicating a wide margin of safety (for the numerical value chosen for the system parameters of this model) for precluding limit cycle operation. For example, if $M = 10D = 2.2 \times 10^{-3}$ and $1/k_F = 1 \times 10^{-7}$, then the lower

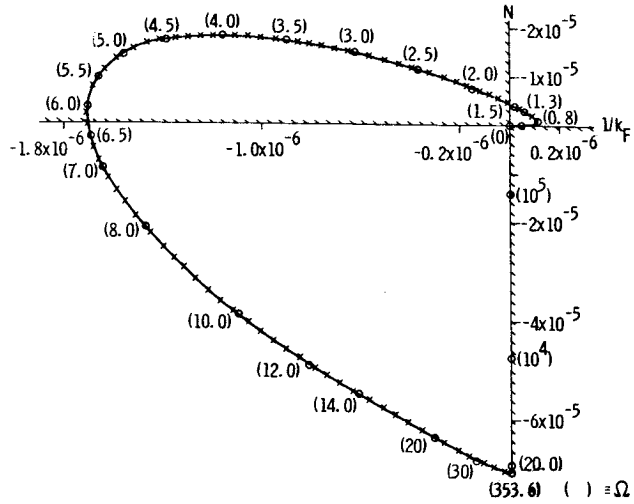

Fig. 5 $1/k_F - N$ parameter plane, Model 2.

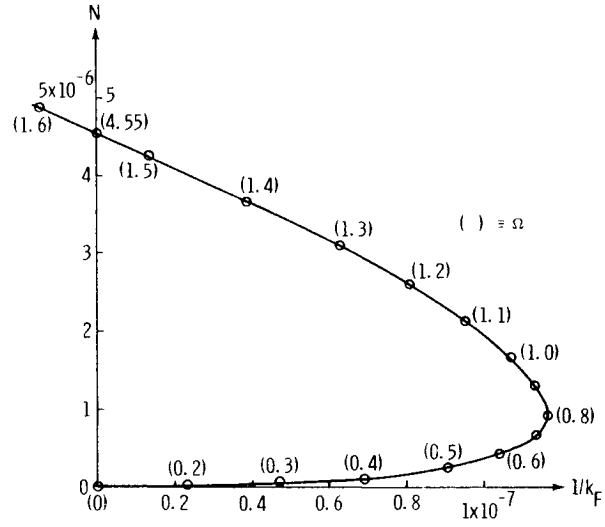

Fig. 6 Limit cycle region of interest on parameter plane, Model 2.

value of N is 0.30×10^{-6} (with a corresponding value of $\Omega = 0.57$) and the upper value is 1.95×10^{-6} (and $\Omega \approx 1.06$). Since D is so small (with respect to unity), the two values of A corresponding to each value of N are [from Eq. (11)]

$$A \approx 4M/\pi N, 0 \quad (19)$$

Thus two of the four indicated limit cycles have negligible amplitudes *(A)* and can be ignored. The other two significant amplitudes, the one corresponding to $N = 0.3 \times 10^{-6}$ being a stable limit cycle ($A^s = 9337$, $\Omega^s = 0.57$) and the other corresponding to $N = 1.95 \times 10^{-6}$ being unstable ($A^u = 1436$, $\Omega^u = 1.06$). These results were not confirmed by analogue simulation. It is felt by the author that they are sufficiently straightforward and do not warrant the effort.

Analysis of Model 3

The model chosen for the CMG and vehicle single-axis dynamics is shown in Fig. 7. The nonlinear relationship (indicated by the symbol N) between gimbal friction torque T_F and gimbal angle δ is portrayed in Fig. 8. The mathematical description, developed by Dahl, of this relation is

$$\dot{T}_f = y \dot{\delta} \quad (20)$$

where

$$y \equiv (dT_f/d\delta) = \gamma (T_f \text{ sgn } \dot{\delta} - T_{GFo})^2 \quad (21)$$

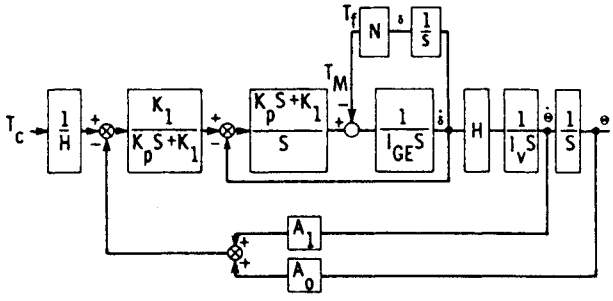

Fig. 7 Model 3.

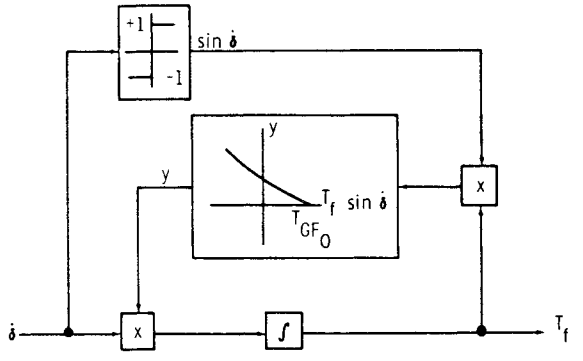

Fig. 8 CMG friction Model (Dahl).

and γ and T_{GFo} are parameters describing the friction relationship[13] and the overdot represents differentiation with respect to time. As in the previous analyses, this analysis was based on using a describing function to represent the nonlinearity N. This in turn was based on the assumption of a sinusoidal input to the nonlinearity of amplitude A and frequency Ω.

Kuo described this nonlinearity by developing a describing function.[14] Instead of using the straight line approximations conventionally used in the derivation of many describing functions, he used the actual curved lines precisely representing Eqs. (20) and (21). Using the complex notation of N,

$$N=N_1+iN_2 \tag{22}$$

where

$$N_1 \equiv (\bar{B}_1/A) \tag{23a}$$

and

$$N_2 \equiv (-\bar{A}_1/A) \tag{23b}$$

Kuo's expressions for $\bar{A}_1$ and $\bar{B}_1$ may be rewritten as functions of the arguments a and T_{GFo}, leading to

$$\bar{A}_1 = -\frac{4T_{GFo}}{\pi}+\frac{1}{\pi A\gamma}\times \ln\left[\frac{(C_2-A)(C_1+A)}{(C_2+A)(C_1-A)}\right] \tag{24a}$$

and

$$\bar{B}_1 = -(2/\gamma A)-\frac{C_2}{\gamma A(C_2^2-A^2)^{1/2}}+\frac{C_1}{\gamma A(C_1^2-A^2)^{1/2}} \tag{24b}$$

where

$$a \equiv 2\gamma A\, T_{GFo} \tag{25}$$

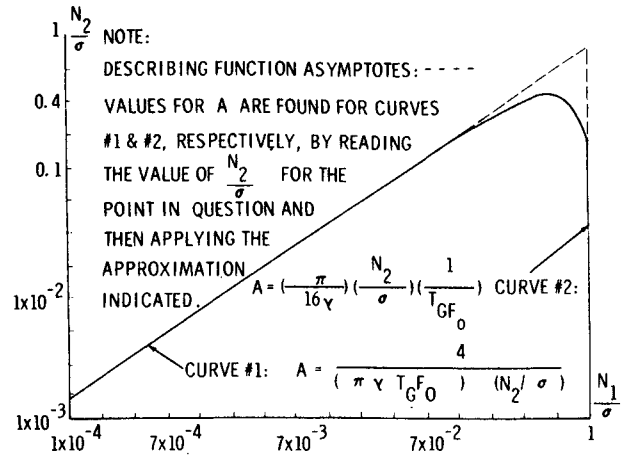

Fig. 9 Normalized Dahl describing function locus.

Approximations for these curves may be obtained by deriving the asymptotes for N_2 vs N_1. The asymptote associated with small vales of $a\,(a \ll 1)$ is

$$N_1 \approx \gamma T^2_{GFo} \tag{26a}$$

and the asymptote associated with large values of $a\,(a \gg 1)$ is

$$N_2 \approx [(4T_{GFo})^{3/4}\gamma^{1/4}/\pi]N_1^{3/4} \tag{26b}$$

The latter expression is simplified if one plots the real (N_1) and imaginary (N_2) parts of the describing function on log-log paper:

$$\log N_2 = \log K + (2/3)\log N_1 \tag{27}$$

where

$$K=(4T_{GFo})^{2/3}\gamma^{1/3}/\pi) \tag{28}$$

Hence one obtains a straight line with a slope of 2/3 and a y-intercept of K for one asymptote and a straight line, parallel to the Y-axis, for the other asymptote. The effect of variations in the gimbal bearing parameters T_{GFo} and γ may now be seen explicitly.

Let k_T be the factor by which T_{GFo} is increased (or decreased), i.e., the new value of T_{GFo} is k_T times as large as the former value. Also let k_γ be the factor by which γ is increased (or decreased). Then, examination of Eqs. (26) shows the effect of altering the numerical values of T_{GFo} and γ is to multiply the former values of N_1 and N_2 (of the describing functions) by the quantity, $k^2{}_T k_\gamma$.

Now, a general map of N_2 vs N_1 may be developed for use in this and future limit cycle investigations for this particular form of nonlinearity. It is universal in the sense that it permits one to choose any value of T_{GFo} and γ and see its effect on the N_2 vs N_1 map, by placing it on an N_1, N_2 parameter plane stability map to predict and analyze limit cycle existence and behavior.

A new parameter is defined:

$$\sigma \equiv \gamma T^2_{GFo} \tag{29}$$

Now, a map of N_2/σ vs N_1/σ is simply obtained by plotting the two straight lines [asymptotes of Eqs. (26)] on Fig. 9.

Values of A may also be found from Fig. 9 by again resorting to approximations. For the asymptote associated with relatively large values of a,

$$N_2 \approx (4T_{GFo}/\pi A) \tag{30}$$

which leads to an expression for A in terms of N_2/σ and parameters γ and T_{GFo}:

$$A \approx \frac{4}{(\pi\gamma T_{GFo})(N_2/\sigma)} \tag{31}$$

Thus for any location on the large a (slanting) asymptote (curve 1, Fig. 9), A may be determined for a given point by looking at the associated value of N_2/σ and using Eq. (31). For the range of numerical values used in the LST analysis, Eq. (31) has proven to be a fairly good approximation.

For the small a (vertical curve 2 on Fig. 9) asymptote, values of A are found by approximating Eq. (24a) with a power series and truncating. Let the natural logarithm term, $(a+a^2+1)^2$, be approximated by the term

$$\mathcal{L} \equiv 2a^2 + 2a + 1 \tag{32}$$

Then a power series expansion of $\ln \mathcal{L}$ is

$$\ln\mathcal{L} = 2\left[\frac{\mathcal{L}-1}{\mathcal{L}+1} + \frac{1}{3}\left(\frac{\mathcal{L}-1}{\mathcal{L}+1}\right)^3 + \ldots\right]$$
$$= \frac{2a(a+1)}{a^2+a+1} + \frac{2}{3}\left[\frac{a(a+1)}{a^2+a+1}\right]^3 + \ldots \tag{33}$$

Combining Eq. (33) with Eqs. (23b) and (24a) leads to an approximation for A as a function of N_2/σ:

$$A \approx (\pi/16\gamma)(N_2/\sigma)(1/T_{GFo}) \tag{34}$$

For LST numerical values, this turns out to be a poor, but barely acceptable, approximation. The problem in approximations arises, for LST numerical parameters, because a difference between two nearly identical numbers is required in Eq. (24a).

Finally, Eqs. (23) and (24) are used to determine the transition curve connecting the two asymptotes. The describing function plot of Fig. 9 may now be used in conjunction with a stability contour, such as will be developed in the next section, on an N_I, N_2 parameter plane. If it is redrawn on a transparency it may be used with a stability map (as will be demonstrated on Figs. 12 and 13) without redrawing it each time by displacing it in both the N_I and N_2 direction by an amount equal to $k_f^2 k_\gamma$. (It has been redrawn on Figs. 12 and 13 for the sake of clarity in this paper.)

As in the previous analyses, the possibility of limit cycle existence will be determined. When it is predicted that one exists, its characteristics will be determined.

The model shown in Fig. 7 may be described in conventional control system form (closed-loop transfer function) as

$$\frac{\theta}{T_c} = \frac{K_I}{I_v I_{GE} s^4 + I_v K_p s^3 + I_v (N+K_I) s^2}$$
$$+ K_I H A_I s + K_I H A_0 \tag{35}$$

The characteristic equation associated with this model is

$$I_{GE} s^4 + [K_p + (N_2/\Omega)s^3 + (K_I + N_I)s^2 +$$
$$K_I K_I s + K_0 K_I = 0 \tag{36}$$

where

$$K_0 \equiv HA_0/I_v \tag{37}$$

and

$$K_I \equiv HA_I/I_v \tag{38}$$

The system described by Fig. 7 appears suitable for describing function analysis because it is low pass and the system parameters are assumed time invariant. A describing function N is used to represent the nonlinearity (herein assumed to be CMG gimbal friction). Recall that for a limit cycle to occur, it is required that all characteristic Eq. (36) roots have negative real parts except for one pair which must be purely imaginary roots. This condition is determined mathematically and, for ease of visualization, is portrayed graphically. In the latter case, two adjustable parameters are selected, N_I and N_2. A correlation between these parameters and the roots of the characteristic equation is determined by mapping the stability contours from the complex s-plane onto the selected (N_I, N_2) parameter plane. For the system under consideration, only one such stability boundary exists and is easily found.

Analysis of Eq. (36) indicates the absence on the N_I, N_2 parameter plane of either a stability boundary associated with the real roots of the characteristic equation or the boundary at infinity.

The simultaneous solution of the nonlinear relation of Eq. (23) and the purely imaginary root boundary yields the condition for a limit cycle, assuming the indicated solution occurs adjacent to a stable region (true in this case). This condition is readily apparent on the parameter plane as the intersection (if one occurs) between the purely imaginary root boundary and the nonlinear locus of Eq. (23). From this point of intersection the frequency (Ω) and magnitude (A) of the indicated limit cycle(s) may be determined as functions of the characteristics of the nonlinearity and of the adjustable parameters. Further, the behavior of each limit cycle when a small perturbation is applied to its amplitude and, hence, the nature of limit cycle stability also are apparent on the parameter plane.

Turning to the characteristic Eq. (36) and setting $s = i\Omega$, one may obtain the real imaginary parts of the equation:

$$-N_I \Omega^2 = -(K_0 K_I - K_I \Omega^2 + I_{GE} \Omega^4) \tag{39}$$

and

$$-N_2 \Omega = -(K_I K_I - K_p \Omega^2) \tag{40}$$

which yields the Jacobian

$$J = \Omega^3 > 0 \; \forall \; \Omega > 0 \tag{41}$$

Solving Eqs. (39) and (40) for the purely imaginary root boundary, one obtains

$$N_I = \frac{I_{GE}\Omega^4 - K_I\Omega^2 + K_0 K_I}{\Omega^2} \tag{42a}$$

and

$$N_2 = \frac{-(K_p\Omega^2 - K_I K_I)}{\Omega} \tag{42b}$$

This boundary (cross-hatched curve) is sketched on Fig. 10, the nature of the Jacobian indicating where the stable region lies. If the nonlinear locus of the describing function defined in Eqs. (22-24) is also drawn on the same $N_I - N_2$ plane, it is seen that several conditions can occur, depending on the numerical values selected for the system parameters. For a fixed set of values for I_{GE}, K_0, K_I, K_I, K_p, either no intersections (or predicted limit cycles) occur (Fig. 11a) or two intersections occur (Fig. 11b). In the latter case one limit cycle is stable (with indicated amplitude and frequency A^s and Ω^s, respectively) and one is unstable (A^u, Ω^u). In that case, if the amplitude (A) of the assumed sinusoidal input to the nonlinearity is always less than A^u, the output of the nonlinearity will asymptotically approach zero. However, if-

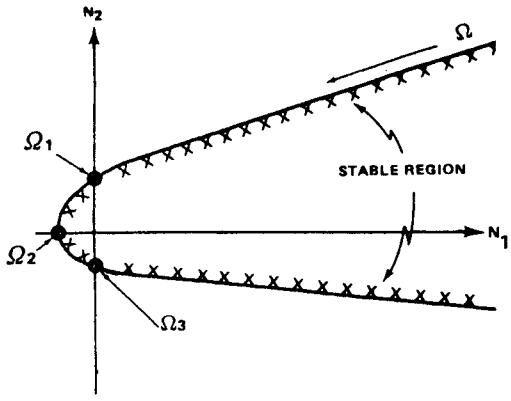

NOTE: $\Omega_1, \Omega_2, \Omega_3$, FOUND FROM EQUATIONS SHOWN.

$$\Omega_1 = \left[\frac{K_1 - \sqrt{K_1^2 - 4I_{GE}K_oK_I}}{2I_{GE}}\right]^{1/2}$$

$$\Omega_2 = \sqrt{\frac{K_I K_1}{K_p}}$$

$$\Omega_3 = \left[\frac{K_I + \sqrt{K_I^2 - 4I_{GE}K_oK_I}}{2I_{GE}}\right]^{1/2}$$

Fig. 10 $N_1 N_2$ parameter plane, Model 3.

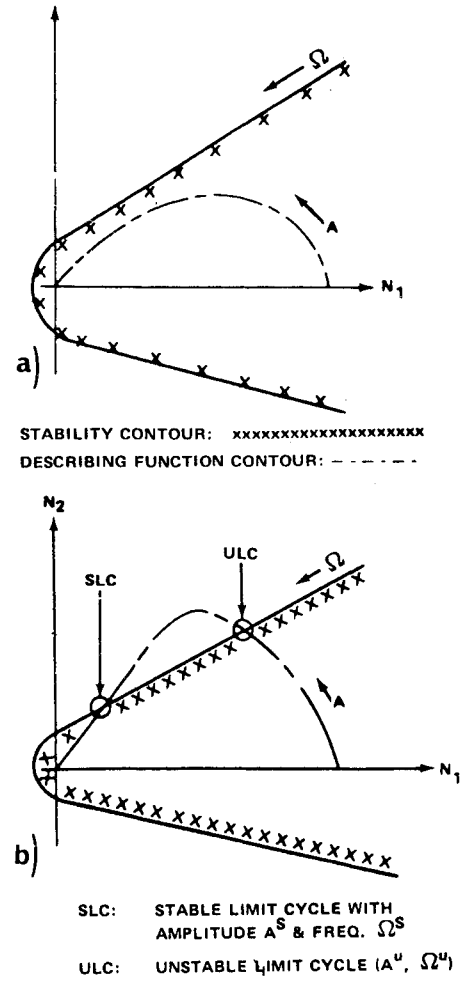

Fig. 11 Parameter plane sketches, Model 3. a) $N_1 - N_2$ parameter plane with no limit cycle. b) $N_1 - N_2$ parameter plane with two limit cycles.

A ever exceeds the value A^u (such as by an initial condition), then A will approach A^s (and Ω will approach Ω^s). In the limiting case where the curves osculate but do not intersect, a single semistable (orbitally semistable) limit cycle is indicated. To interpret these phenomena physically, one may refer to Fig. 7. The input to the nonlinearity is δ. For describing function analysis, it is assumed to be sinusoidal and of the form of Eq. (1), i.e.,

$$\delta = A \sin \Omega t \tag{43}$$

The output of the nonlinearity, T_f, is then assumed to be of the form

$$T_f \approx N\delta = (N_1 + iN_2)\delta = N_1\delta + (N_2/\Omega)\dot{\delta}$$
$$= N_1 A \sin \Omega t + N_2 A \cos \Omega t$$
$$= A(N_1^2 + N_2^2)^{1/2} \sin(\Omega t + \phi), \phi = \tan^{-1}(N_2/N_1) \tag{44}$$

This is in the form of Eq. (2). Using Eq. (43) and (44) with the relations shown in Fig. 7, one may now obtain the values of the other variables (e.g., θ and $\dot{\theta}$) when $T_c \equiv 0$ and a limit cycle is predicted. Typical numerical values of LST were altered slightly, because of the passage of time between analyses, and are shown in Table 3 (slightly different from Table 1). They are described in Ref. 15.

The curve for the purely imaginary root boundary is found by substituting numerical values from Table 3 into Eqs. (42). If Table 3 values of γ and T_{GFo} are used for the nonlinear locus representing the friction [Eqs. (22-24)], it is seen that no intersections between the two curves will occur (Fig. 12). (This is the case portrayed in the sketch of Fig. 11a.) Hence no limit cycles are predicted and stable operation is predicted.

If the asymptotes are also plotted on Fig. 12, one sees that, if during the design evolution γ and/or T_{GFo} are increased, the case shown in the sketch of Fig. 11b will occur. In that case two limit cycles are predicted, one stable and one unstable. One such example is shown in Fig. 13, where γ is increased to a value of 1.477×10^6. The unstable limit cycle has a predicted amplitude of 1.0×10^{-6} rad and frequency of oscillations of 2.8 rad/sec. The stable limit cycle amplitude is 2.1×10^{-5} rad with a frequency of oscillation of 5.2 rad/sec. Practically, this means that if A has an initial value that is greater than 4.0×10^{-6} rad it will always converge to a value of 2.1×10^{-5} (the stable limit cycle). However, if the value of A is never permitted to exceed 1.0×10^{-6} rad (the unstable limit cycle), no limit cycle operation will occur and the system will be asymptotically stable.

The foregoing predictions also were confirmed with a simulation on an EAI 231R-V analog computer sufficiently close to confirm the predicted value within the limits of

Table 3 Revised numerical values for LST

Parameter	Numerical Value
A_0	2×10^4 (rad—s)$^{-1}$
A_I	3×10^3 (rad)$^{-1}$
H	271 Nmsec (200 ft-lb-sec)
I_{GE}	5.012 Nmsec^2 (3.7 ft-lb-sec^2)
I_v	1.354×10^5 Nmsec^2 (10^5 ft-lb-sec^2)
K_I	1.354×10^4 Nm (10^4 ft-lb)
K_p	379 Nmsec (280 ft-lb-sec)
T_{GFo}	0.271 Nm (0.2 ft-lb)
γ	1.477×10^5 (Nm rad)$^{-1}$ [2×10^5 (ft-lb rad)$^{-1}$

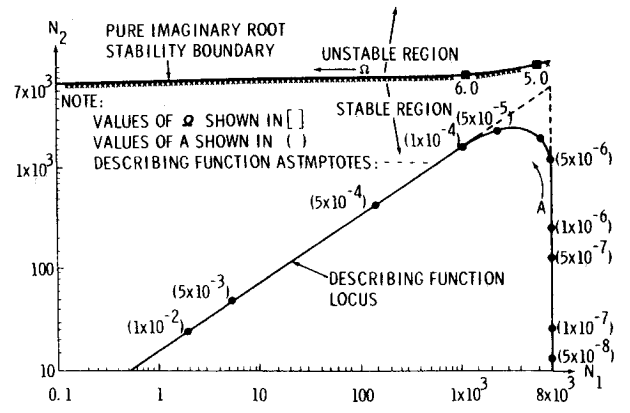

Fig. 12 N_1-N_2 *parameter plane* ($\gamma=1.477\times10^5$), **Model 3.**
a) N_1-N_2 **parameter plane with no limitcycle.**
b) N_1-N_2 **parameter plane with two limit cycles.**

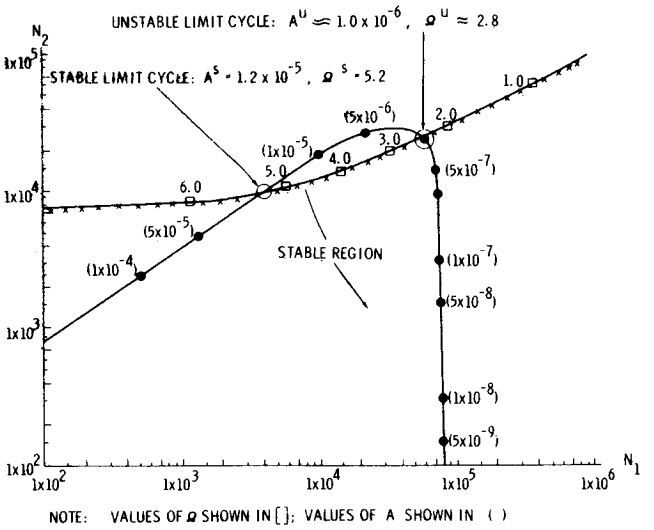

Fig. 13 N_1N_2 **parameter plane** ($\gamma=1.477\times10^6$), **Model 3.**

describing functions analysis assumptions. A summary of the analytical predictions and simulation results is given in Table 4. Hence for the single nonlinearity considered, i.e., the output gimbal friction relation developed by Dahl, no limit cycle is predicted for presently estimated LST numerical parameters. However, if the design characteristics of the LST CMGs should allow numerical values of γ and/or T_{GFo} substantially larger than those indicated in Table 3, two limit cycles will occur, one stable, one unstable.

This analysis has considered neither the effect of multiple nonlinearities nor the effect of sampling (such as will be performed by an onboard digital computer). A sampled data analysis is now underway to consider the latter.

Comparison of Results

Based on preliminary hardware measurements it presently appears that the Dahl model (included in Model 3) provides a basic description of the nonlinear friction characteristic associated with the CMG output gimbal. If one were to plot gimbal friction torque vs gimbal angle, for instance, the basic curve would be in approximate agreement with the CMG hardware measurements now being obtained. Certain anomalies are being measured but have not yet been verified or explained. Hence, for the present, the author feels that the Dahl model is the best available friction model for use in dynamic analysis. If indeed the anomolies turn out to be significant, the present Dahl model will have to be modified. This means that a new mathematical description of the nonlinearity will then have to be developed if an analysis is to be performed similar to those reported in this paper. Even in that case the design insight obtained by investigating the dynamic effects of the present Dahl model will be valuable, since at the minimum it appears to provide an approximate description of the actual behavior. For instance, the effect of varying friction model parameters γ and T_{GFo} is shown explicitly.

The modified Sperry friction model (included in Model 2) essentially is a piecewise-linear simplification of the Dahl model. For instance, as the gimbal angle increases from a zero force position, the friction torque increases with a constant slope K_F which is comparable to the initial slope of $\sigma=\gamma T_{GFo}^2$ of the Dahl model. Whereas in the Sperry model the friction torque continues (until amplitude T_{GFo} is reached) to increase at a constant slope as the gimbal angle increases, in the Dahl model it gradually levels off to a value of T_{GFo}.

The Bendix model (Model 1) is an older attempt to characterize the friction nonlinearity. The idea was to (see Fig. 2) show that the output gimbal doesn't rotate (but does deform elastically at a rate m) until the commanded gimbal angle exceeds a certain value (D) at which time the gimbal breaks away and then moves with a constant slope κ.

Comparison of the three friction models is in order. If experimental measurements actually confirm the Dahl model or a modification thereof (and preliminary results indicate this will be the case), then the results reported herein for Model 3 either are directly applicable or a modification of the friction model would make them applicable. Since Model 2 is a piecewise-linearization of Model 3 for small gimbal angles, it is also appropriate for analysis. However, if the Dahl model proves to be a reasonably accurate representation of the gimbal friction torque, it is preferable to Model 2 since no approximations are made. Model 1 appear to be an inaccurate representation and also should be replaced in future work by the Dahl model.

The incorporation of the three friction models into models of the LST single axis dynamics was performed sequentially. Consequently the LST models and the numerical values of their parameters have changed and the three are not directly comparable. However, it is shown that conditions for limit cycle behavior can be specified for each of the three models.

Conclusions

For numerical values considered to be representative of the LST and its CMGs, analysis indicates (and analog simulation confirms) the absence of limit cycle behavior due to the CMG output gimbal friction nonlinearity. Because of the present early stage of development of the LST, it is expected that the numerical values (and indeed mathematical characterization

Table 4 Summary of model 3 results

		Analytical Predictions		Simulation Results			
γ (Nm rad)$^{-1}$ [(ft-lb rad)$^{-1}$]	Limit cycle	A (rad)	Ω(rad/sec)	A (rad)	Ω (rad/sec)	θ(rad)	$\dot{\theta}$ (rad/sec)
$1.477\,(2\times10^5)$	No						
$1.477\,(2\times10^6)$	Unstable	1.0×10^{-6}	2.8	2.0×10^{-7}	2.4	1.6×10^{-9}	4×10-9
$1.477\,(2\times10^6)$	Stable	2.1×10^{-5}	5.2	1.5×10^{-6}	5.2	7.5×10^{-7}	

of CMG friction models) will change. Because of this, a wide spread of numerical values of actual variations in friction parameters has been examined. Further, a general technique of analysis of such systems has been specified and used in great detail. This technique should be applicable to future alterations in the LST. As such, it provides a design tool for enhancing the efficiency of large scale computer simulation by predicting dynamic responses (thus aiding in the time-consuming debugging process) and in helping to select numerical values to be incorporated in the simulations.

The Dahl model appears to be the most accurate existing mathematical represenation of the nonlinear friction torque phenomenon associated with the CMG output gimbal. Tests on CMG hardware are underway to determine accurately this phenomenon. Preliminary results indicate that the Dahl model, or perhaps a modification of it, is a good representation of the physical phenomenon. If that is verified, the Dahl model will be preferable to the other models used in this report. It is shown that the Dahl model can be cast in describing function form and easily used for analytical limit cycle predictions.

The analyses do not include the dynamic effects caused by implementing the control with a digital computer. Sampling and quantization must also be considered when one predicts or attempts to obviate limit cycles. However, an understanding of each phenomenon (such as the dynamics associated with the friction nonlinearity) greatly assists the control system designer in his efforts to cope with the dynamic effects of each. Hence the motivation for analyzing the limit cycle behavior caused by the friction nonlinearity with a simple, continuous-data, single axis, rigid body model.

References

[1] Sandhu, G. S., "Rigid Body Mode Pointing Accuracy and Stability Criteria for an Orbiting Spacecraft," *Journal of Spacecraft and Rockets,* Vol. 11, No. 8, Aug. 1974, pp. 599-601.

[2] Seltzer, S.M., "Analysis of a Control System Containing Two Non-linearities," *International Journal of Control,* Vol. 10, No. 2, Feb. 1970, pp. 1058-1064.

[3] Connell, G.M., "A Method of Earth Pointing Attitude Control for Elliptic Orbits," *AIAA Journal,* Vol. 10, No. 3, March 1972, pp. 258-263.

[4] Schiehlen, W., "Comment on a Method of Earth-Pointing Attitude Control for Elliptic Orbits," *AIAA Journal,* Vol. 11, No. 1, Jan. 1973, p. 127.

[5] Rybak, S.C., "Research and Applications Module (RAM) Phase B Study: Free Flyer GN&C Trade Study Report," RAM-B-GNC-407, Oct. 1971, Bendix Corp., Denver, Colo.

[6] Rybak, S.C., "High Accuracy Stabilization and Control," Tech. Rept. MT-2383, Bendix Corp., Denver, Colo. Dec. 1971.

[7] Frieder, M., "A Note on CMG Characteristics and Spacecraft Limit Cycling," Engineering File MT-15, April 1972, Bendix Corp., Teterboro, N.J.

[8] Andronow, A. and Chaikin, S., *Theory of Oscillations,* Princeton University Press, Princeton, N.J., 1949, pp. 203-208.

[9] Ogata, K., *Modern Control Engineering*, Prentice-Hall, Englewood Cliffs, N.J., 1970, pp. 585-587.

[10] Gelb, A., and Vander Velde, W. E., *Multiple-Input Describing Functions and Non-Linear Systems Design*, McGraw-Hill, New York, 1968.

[11] Siljak, D.D., *Nonlinear Systems,* Wiley, New York, 1969, pp. 152-171, 177-186.

[12] Seltzer, S.M., "CMG-Induced Dynamics," TM X-64833, Feb. 1974, NASA.

[13] Dahl, P.R., "A Solid Friction Model," TOR-158 (3107-18), The Aerospace Corp., El Segundo, Calif., May 1968.

[14] Kuo, B.C., Seltzer, S.M., and Singh, G., "Stability Study of the Large Space Telescope (LST) System with Nonlinear CMG Gimbal Friction," AIAA Paper 74-874, Anaheim, Calif., 1974; submitted for publication in the *Journal of Spacecraft and Rockets.*

[15] Liden, S.P., "Precision CMG Control for High-Accuracy Pointing," *Journal of Spacecraft and Rockets,* Vol. 11, No. 4, April 1974, pp. 236-240.